CHIN. PHYS. LETT. Vol. 29, No. 7 (2012) 078103

Effect of Grain Boundary on Spinodal Decomposition Using the Phase Field Crystal Method *

YANG Tao(杨涛)**, CHEN Zheng(陈铮), ZHANG Jing(张静), DONG Wei-Ping(董卫平), WU Lin(伍林)

State Key Laboratory of Solidification Processing, School of Material Science and Engineering, Northwestern Polytechnical University, Xi'an 710072

(Received 11 May 2012)

Spinodal decomposition (SD) with different grain boundaries (GBs) is investigated on the atomic scale using the novel phase field crystal model. It is demonstrated that the decomposition process is initiated by precipitating one phase with a larger lattice constant in the tension region at the GBs and the other one with a smaller lattice constant in the compression region. As the phase separation proceeds, the dislocations comprising the low-angle GBs migrate toward the compositional domain boundaries to relieve the coherent strain energy, and eventually become randomly distributed in the coarsening regime of SD, which leads to the disappearance of the low-angle GBs. For high-angle GBs, the location of GBs remains unchanged, while the atoms rearrange along the GBs to fit the stress field arising from compositional inhomogeneity.

PACS: 81.05.Bx, 61.72.Mm, 81.30.Mh, 81.10.−h DOI: 10.1088/0256-307X/29/7/078103

Spinodal decomposition (SD) occurs by the spontaneous amplification of compositional domains when a homogenous phase is quenched into the unstable region of the phase diagram. As a common strengthening mechanism for alloys, SD has attracted an extensive attention among researchers; see Ref. [1] for a review. In recent years, great efforts have been devoted to studying SD in the presence of various defects.[2−9] For instance, studies on the coupling between phase separation and dislocations[3−6] indicated that apart from enhancing the SD process,[3,4] the dislocations would migrate to the compositional domain walls to relieve the coherent strain energy built up during the SD process.[5,6] Similarly, the effect of GBs has been investigated by using computational methods.[7−9] Liu *et al.*[7] demonstrated that phase aggregation is preferred at the GBs with no formation of a particular pattern, while the grain grows slowly through migration of the GBs by applying the Monte-Carlo method. Yet, it was discovered with a continuum phase field approach by Ramanarayan and Abinandanan[8,9] that the primary effect of GBs is the formation of alternating bands of product phases parallel to the boundary and in the same time grain growth is effectively suppressed by the bands. Also, these previous works fail to reflect the information on the atomic scale, which is of great importance in understanding the interplay between defects and phase separation. Given this, gaining a comprehensive knowledge of the SD with GBs is still worth exploring.

The purpose of this work is to explore the effects of GBs on SD on the atomic scale from two aspects of low-angle GBs (LAGBs) and high-angle GBs (HAGBs). The phase-field crystal (PFC) approach[10−12] adopted here is a new extension to the traditional phase-field method, which automatically combines many physical features, including elastic effects and crystal anisotropies due to the periodic nature of the density field, while addressing issues of the interfaces, dislocations and other lattice defects.[11−14] The PFC approach also has advantages over other traditional microscopic techniques, such as molecular dynamics, because it operates on diffusive time scales making the long-time behavior and large-scale structures accessible. The final dimensionless form is given by

$$F = \int d\boldsymbol{x}\Big\{\frac{n}{2}[B^l + B^s(2R^2\nabla^2 + R^4\nabla^4)]n - \frac{t}{3}n^3 + \frac{v}{4}n^4 + r\delta N + \frac{w}{2}\delta N^2 + \frac{u}{4}\delta N^4 + \frac{L^2}{2}|\nabla\delta N|^2\Big\}, \quad (1)$$

where n and δN represent the reduced density field and concentration field, respectively. The interatomic distance R may be tuned by changing parameters R^0 and R^1 through the approximation $R = R^0 + R^1 \cdot \delta N$. B^l and B^s are the dimensionless bulk modulus of the liquid state and the crystalline phase given by $B^s = B^{s,0}$ and $B^l = B^{l,0} + B^{l,2} \cdot (\delta N)^2$, where the parameters R^0, R^1 and $B^{l,0}$, $B^{l,2}$, $B^{s,0}$ are the coefficient parts of variables R, B^l and B^s in Taylor's expansions, respectively. The tendency towards liquid/solid phase separation is controlled by w while the length scale of the precipitates is determined by the interaction of L and w. Parameters u, t, v and r are model constants defined by Elder *et al.*[12]

*Supported by the National Natural Science Foundation of China under Grant Nos 51174168, 51075335 and 10902086, the Graduate Starting Seed Fund of NPU under Grant No Z2012025, and the NPU Foundation for Fundamental Research under Grant Nos JC201109 and JC201005.

**Corresponding author. Email: 420929211@163.com

© 2012 Chinese Physical Society and IOP Publishing Ltd

The dynamic equations for the fields δN and n are considered by assuming a substitutional diffusion between two species and the mobility coefficient being a constant. In this limit, the motion equations can be written in the form

$$\frac{\partial \mathrm{n}}{\partial t} = M_e \nabla^2 \Big\{ nB^l + \frac{1}{2} B^s (2R^2\nabla^2 + R^4\nabla^4)n + vn^3 - tn^2 + \frac{B^{\mathrm{s}}}{2}[2\nabla^2(nR^2) + \nabla^4(nR^4)] \Big\}, \quad (2)$$

$$\frac{\partial(\delta N)}{\partial t} = M_e \nabla^2 \Big\{ B^{\mathrm{l},2} n^2(\delta N) + 2nB^s R R^1 \nabla^2 n + r + w(\delta N) + 2nB^s R^3 \mathrm{R}^1 \nabla^4 n + u(\delta N)^3 - L^2\nabla^2(\delta N) \Big\}. \quad (3)$$

An operator splitting algorithm is used to solve Eqs. (2) and (3) proposed by Tegze *et al.*[15] on a 512×512 computational domain with periodic boundaries in both directions. The grid size and time step are set to be $\Delta x = 1.1$ and $\Delta t = 1.5$. The phase diagram[12] corresponding to Eq. (1) can be calculated for the parameters $R^0 = 1$, $R^1 = 0.25$,$B^{l,2} = -1.8$, $B^{s,0} = 1$, $L = 2.65$, $u = 4$, $w = 0.088$, $t = 0.6$, $v = 1.00$, $r = 0$ as shown in Fig. 1. The spinodal decomposition line is added into the phase diagram according to the relationship of the free energy and the composition $\partial^2 F/\partial(\delta N)^2 < 0$.

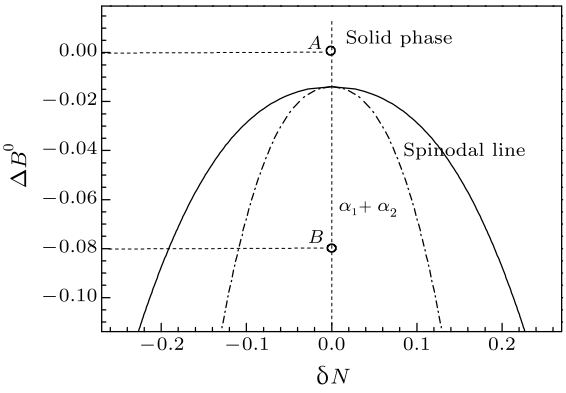

Fig. 1. Phase diagram of the binary crystal phase field model.[12] The spinodal curve (dotted line), supposed boundary between metastable and unstable states, is characterized by $\partial^2 F/\partial(\delta N)^2 < 0$.

The initial condition used to simulate grain boundaries is constructed as follows. Two solid slabs, which are rotated by an angle $\theta/2$ in opposite directions, are placed into a supercooled liquid, where $\delta N = 0$ as indicated by point A in Fig. 1. The solid with two-dimensional hexagonal symmetry can be created using the one-mode approximation for density field, i.e., $n = A[0.5\cos(2qy/\sqrt{3}) - \cos(qx/\sqrt{3})]$, where $q = \sqrt{3}/(2R)$ and $A = 4(t + \sqrt{t^2 - 15v\Delta B})/15v$. The system is then evolved for a long time to achieve equilibrium before the SD simulation is performed. It is worth noting that due to the periodic boundary conditions and the symmetries, there are always two equivalent grain boundaries in the simulation cell. Therefore, part of the left GBs in the simulation box are shown, with the initial structures before the quench shown in Fig. 2. To facilitate the analysis of GB effects, defect sites with a surrounding atom number other than 6 are highlighted by black dots, as shown in Figs. 2(c) and 2(f). According to the atom configurations, the left tilt LAGB is composed by the positive edge dislocations, as shown in Fig. 2(a), implying a tensile stress region on the upper half of each dislocation and a compressive region on the lower. Remarkably, the dislocations composed of the LAGBs are not strictly located in the same line along the GB, as shown in Fig. 2(c). However, this slight difference has an important impact on the early stage of morphological evolution.

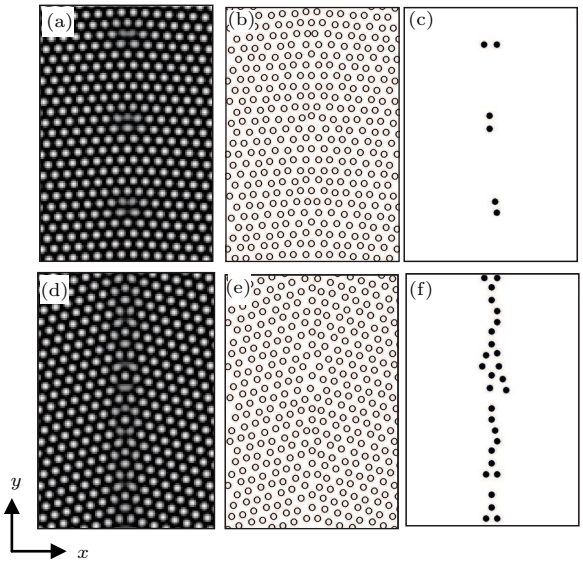

Fig. 2. Snapshots of the left GBs in the simulation box. The gray scales in the figure correspond to density field n for tilt GBs with misorientation $\theta = 8°$ (a, b, c) and $\theta = 30°$ (d, e, f). The schematic diagrams for atom configurations are shown in (b) and (e), corresponding to (a) and (b), respectively. To facilitate the analysis, density field n is simplified by denoting the defect cores with black dots as in (e) and (f).

The simulation of SD with LAGBs is initiated by quenching the alloy from point A (Fig. 1) to point B, shown in Fig. 3, where the black and white colors illustrate solute-enriched and solute-depleted regions, respectively. In order to elucidate the interactions of GBs and SD, the concentration field δN is superimposed on the corresponding simplified density field n. Within a very short time, t=1200, solute atoms enrich themselves in the tensile stress region of each dislocation and deplete in the compressive region, producing a special structure as shown in Fig. 3(a). This is because in this model, the atomic distance in the solute-rich region is larger than that in the solute-poor region according to the equation $R = R^0 + R^1 \cdot \delta N$, producing the compression stress in the former region and the tension stress in the latter around the coherent

domain boundaries. In the sense of relaxing the elastic strains, the solute-rich region is favored in the tensile stress field of dislocations, as shown in Fig. 4(a). From Fig. 3(b), it can be seen that the clusters tend to grow in one direction normal to GB instead of two, which is the result of asymmetric stress distribution caused by the subtle difference of dislocation locations mentioned earlier. As phase separation proceeds, the clusters grow both in size and concentration in which the latter leads to an accumulated elastic stress field near the phase interfaces. At $t = 15200$, the dislocations begin to depart due to the increasing stress and the GBs become unstable. In the mean time, the interior of the grain undergoes the normal SD, which is much slower than GB-assisted SD. At $t = 25200$, the GB-assisted clusters reach their respective equilibrium compositions with the formation of solute-rich blocks separated by solute-poor regions, as shown in Fig. 3(d). In this process, the dislocations move further toward the compositional domain boundaries to relieve the built-up strain energy. At present, the profile of the dislocations is in a relatively regular order with most dislocations on the interfaces which are parallel to x direction. At $t = 50200$, the system evolves into the coarsening regime in which the normal SD in the grain interior becomes connected with GB-assisted phases, as shown in Fig. 3(e). With the progression of the coarsening process, the pattern of GB-assisted phases formed in the earlier time starts to disappear, causing the dislocations to become disordered.

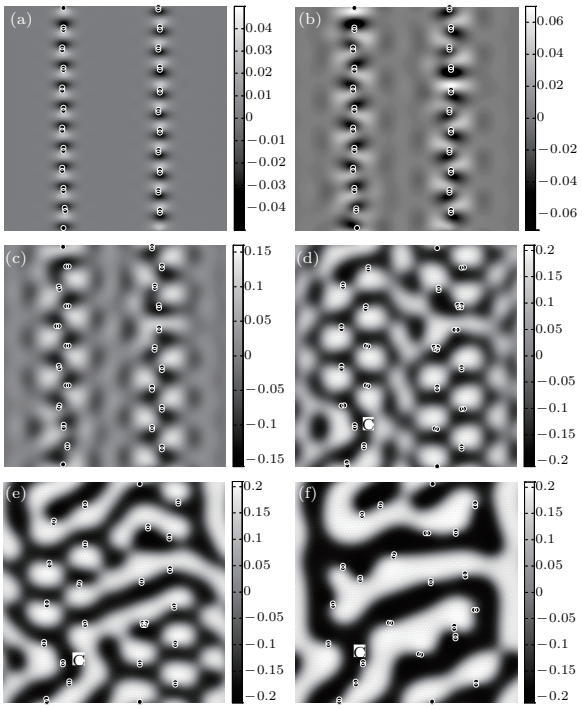

Fig. 3. Evolution of the concentration field with LAGB of $\theta = 8°$, superimposed on the corresponding density field. The time sequence (a)–(f) corresponds to $t = 1200$, 9200, 15200, 25200, 50200, 99200, respectively.

Notably, it can be concluded from Figs. 3(d)–3(f) that the dislocations not only glide along the phase interfaces, but also across the precipitates, as shown by the dislocation marked with letter C. In the spirit of greater strain relief, the dislocations situated on the side of compositional domain boundaries (Fig. 3(d)) tend to moving to the interfaces (Fig. 3(f)) with a smaller angle with respect to the x direction, as explained by Fig. 4.

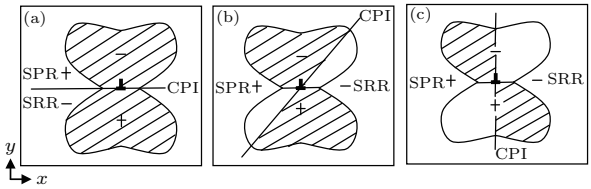

Fig. 4. Schematic illustration of the normal stress fields for the edge dislocation and the coherent phase interface (CPI). Three CPIs with different angles between the x axis from 0° to 90° are displayed in (a)–(c). Here SRR and SPR are the abbreviations for solute-rich region and solute-poor region, respectively. The area enclosed by slashes implies the amount of counterbalancing between the stress fields induced by the dislocation and the composition inhomogeneity. The sign + represents the tension stress while − denotes the compression stress.

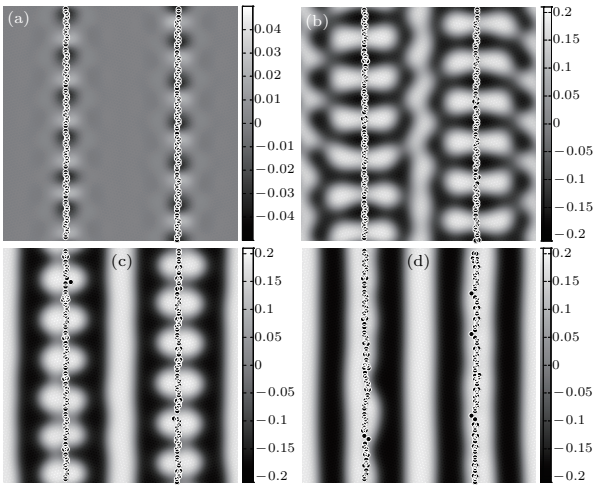

Fig. 5. Evolution of the concentration field with the HAGB of $\theta = 30°$, superimposed on the corresponding density field. The time sequence (a)–(d) corresponds to $t = 3900$, 30000, 62400, 99300, respectively.

The microstructural evolution depicted in Fig. 5 shows the decomposition process for bicrystals with misorientation $\theta = 30°$. Comparing Figs. 3 and 5, it can be concluded that there are two distinct differences between them. First, the location of the GBs remains the same during the phase separation process, demonstrating the better stability of HAGBs. Nevertheless, with a closer observation, the structure of GBs is found to change as the aging progresses, which results from the external stress field of compositional domain boundaries. Second, due to the stability of GBs, the precipitates exhibit a regular morphological

evolution. In the early stage of SD, the solute atoms enrich themselves in the tensile stress region of GBs and form the horizontal short stripe phases, as shown in Figs. 5(a) and 5(b). Within the coarsening regime, the short stripes evolve to circles, then to long stripes parallel to GBs driven by the reduction of interfacial energy.

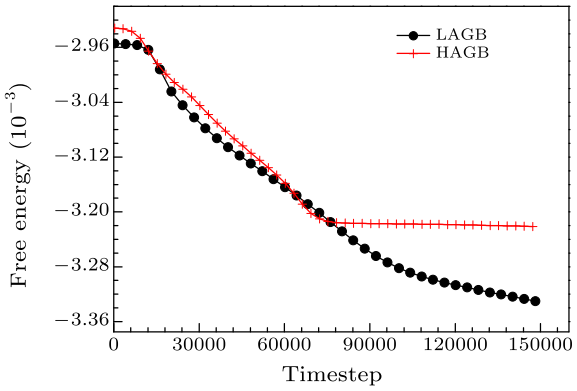

Fig. 6. Plots of free energy against t for systems with different GBs.

In Fig. 6 we show the plots of total free energies as functions of dimensionless time for the simulations shown in Figs. 3 and 5. The total energy for HAGBs experiences a more regular decrease with the slope nearly unchangeable, then remains invariant in time as shown in Fig. 5(d). This is expected due to the relatively high stability of HAGBs, which leads to a weaker influence on the SD. For LAGBs, the total energy starts to decrease rapidly around $t = 11000$ in response to the first appearance of destabilization of GBs. Note the small variance of its slope with time, which can be rationalized in terms of the coupling between the dislocations and compositional domain boundaries.

In conclusion, the dislocations on the LAGBs migrate to the compositional interfaces during the decomposition to relieve the coherent strain energy, which eventually leads to the disappearance of GBs. HAGBs behave in a feature of the high stability that the location of GBs remains unchanged in the phase separation process. Yet, to the end of the strain relief, atoms on the GBs simultaneously rearrange as the aging proceeds. With respect to the morphological evolution, LAGBs show a great influence on the pattern of precipitates in the early stage of SD while HAGBs have an impact throughout the process.

References

[1] Kostorz G 2001 *Phase Transformations in Materials* (Weinheim: Wiley-VCH) chap 6 p 409
[2] Hu S Y and Chen L Q 2004 *Acta Mater.* **52** 3069
[3] Rodney D, Bouar Y Le and Finel A 2003 *Acta Mater.* **51** 17
[4] Li Y S, Li S X and Zhang T Y 2009 *J. Nucl. Mater.* **395** 120
[5] Haataja M and L éonard F 2004 *Phys. Rev.* B **69** 081201
[6] Haataja M, Mahon J, Provatas N and L éonard F 2005 *Appl. Phys. Lett.* **87** 251901
[7] Liu J M, Lim L C, Wu Z C, Cao G H, Chen G and Liu Z G 2000 *J. Mater. Sci.* **35** 2729
[8] Ramanarayan H and Abinandanan T A 2003 *Acta Meter.* **51** 4761
[9] Ramanarayan H and Abinandanan T A 2003 *Physica* A **318** 213
[10] Elder K R, Katakowski M, Haataja M and Grant M 2002 *Phys. Rev. Lett.* **88** 245701
[11] Elder K R and Grant M 2004 *Phys. Rev.* E **70** 051605
[12] Elder K R, Provatas N and Berry J, Stefanovic P and Grant M 2007 *Phys. Rev.* B **75** 064107
[13] Berry J, Elder K R and Grant M 2008 *Phys. Rev.* B **77** 224114
[14] Provatas N, Dantzig J A, Athreya B, Chan P, Stefanovic P, Goldenfeld M and Elder K R 2007 *JOM* **59** 83
[15] Tegze G, Bansel G, Tóth G I, Pusztai T, Fan Z and Gránásy L 2009 *J. Comput. Phys.* **228** 1612